

マイクロ波帯ワイヤレスアクセスにおけるハイトゲインモデルの検討

New Method for Evaluating Height Gain at Subscriber Station for Wireless Access Systems in Microwave Band

北 直樹[†]
Naoki KITA

山田 渉[†]
Wataru YAMADA

佐藤 明雄^{††}
Akio SATO

[†] 日本電信電話株式会社 NTT アクセスサービスシステム研究所
NTT Access Network Service Systems Laboratories, NTT Corporation

^{††} 東京工科大学 コンピュータサイエンス学部
School of Computer Science, Tokyo University of Technology

1. INTRODUCTION

Broadband wireless access (BWA) systems have been drawing a great deal of attention concerning broadband wireless access services such as wireless Internet access that provide tens of megabits per second or higher transmission speeds to users [e.g., 1]. There is a wide spectrum for BWA systems at millimeter-wave frequencies, but the technology is not sufficiently mature to make these systems cost-effective for mass users, and a reliable non-line-of-sight (NLOS) operation is desired to extend the applicable area of fixed wireless access (FWA) systems. Therefore, research on the microwave band BWA system and its propagation channel characteristics is a topic of great interest (e.g., [2]-[4]).

The propagation models for FWA or nomadic wireless access (NWA) systems must be more accurate in regard to the dependency on local conditions around subscriber stations (SSs) than models for mobile communication systems. The reason for this is that the propagation conditions between a base station (BS) and a SS are strongly influenced by the local conditions of the SS because the SS is stationary (or at least has very limited mobility) in the FWA or NWA scenarios. There is of course the ray-tracing propagation model, which represents the best site-specific modeling method [e.g., 5], but this model generally requires a very long calculation time and huge digital terrain and building databases. Therefore, a model is required that is simpler and that can take into consideration the local conditions of the SS.

Modeling of the variation in height of the SS antenna with respect to the path loss (simply referred to as “height variation of the path loss at a SS” hereafter) is an important issue in the design of wireless access systems. The model must take into consideration the local conditions around the SS. Here, the local conditions around a SS mean the building height, road width around the SS, and the distance between the BS and SS. There have been studies such as [6], [7] on this height variation of the path loss at a SS for radio communication system design. However, most of these studies deal with the UHF band up to 2 GHz and focus on mobile communication systems (not FWA or NWA systems). So, the SS antenna height is limited to approximately 3 m (in [6]), and the range of the BS-SS separation is limited to more than 1 km (in [7]) in these models. The height variation of the path loss at a SS for locations higher than 3 m is important for FWA scenarios in which the SS antenna is established on a rooftop or on a wall of a building. In addition, predicting the path loss and height variation of the path loss at a SS in the near region (BS-SS separation of less than 1 km) is important. The path loss prediction in not only the far region in order to estimate the limit of the radio zone, but also that in the near region in order to estimate the achievable transmission speed within the radio zone are necessary because the transmission speed varies depending on the received signal strength according to an adaptive modulating function in modern wireless communication systems such as IEEE802.11 wireless LAN (Local Area Network) systems [8] or IEEE802.16 wireless MAN (Metropolitan Area Network) systems [9] used in wireless access systems.

Although some publications reported some measurement examples for the height variation of the path loss at a SS for microwave band BWA systems [10], [11], these did not propose a model for estimating the height variation of the path loss at a SS.

This paper proposes a height variation model of the path loss for evaluating height gain at a SS in the microwave band. The model takes into consideration the local conditions around a SS and the horizontal distance between the BS and SS. The target area of the model is a fairly homogeneous propagation environment such as a residential area, which is an important service area for wireless access services.

Section 2 describes the characteristics of the height variation of the path loss and height gain at a SS based on measurement results in real environments. Section 3 presents the analysis of the mechanism for the dependency of height variation of the path loss at a SS on the location based on geometrical optics (GO) and the uniform geometrical theory of

diffraction (UTD) [12]. In Section 4, the modeling of the height variation of the path loss at a SS taking into consideration the local conditions around the SS will be presented, and validation of the model in terms of height gain with measured height variation of the path loss at the SS in the microwave band carried out in a residential area in Tokyo and in Ibaraki prefecture in Japan will be presented. Finally, we present our conclusions in Section 5.

2. HEIGHT VARIATION CHARACTERISTICS OF PATH LOSS AT SS IN REAL ENVIRONMENT

The measurements for the height variation of the path loss at a SS were carried out in the Suginami area in Tokyo. The SS antenna height (h_{SS}) was changed from 4.5 m to 10.5 m continuously during measurement at each measurement point using a flexible pole set on top of the van as shown in Fig. 1 and Picture 1. The area is flat. The average height of the buildings in the area is approximately 7.5 m, but some apartment buildings are higher than 10 m.

Typical examples of the acquired height variation characteristics of the received level are shown in Figs. 2(a) and 2(b). Figures 2(a) and 2(b) correspond to the measured results when the BS-SS separation distance is relatively short (330 m) and relatively long (1360 m), respectively. The plots in both figures represent 1-m high section mean values of the acquired data at 5.2 GHz / CW. The BS antenna height is 32 m. The propagation path between the BS and SS is line-of-sight (LOS) and Non-LOS (NLOS) when the SS antenna height is 10 m and 5 m in both figures. The difference in the height variation characteristics of the received level between Figs. 2(a) and 2(b) is clear. The slope of the level attenuation due to a decrease in the SS antenna height is small in Fig. 2(a) compared to that in Fig. 2(b). The difference in the received level between the SS antenna height of 10 m (LOS) and 5 m (NLOS) is 11 dB and 19 dB in Figs. 2(a) and 2(b), respectively. It seems that the slope of the level attenuation due to a decrease in the SS antenna height becomes relatively small in the near region (BS-SS separation is relatively short) compared to that in the far region (BS-SS separation is relatively long).

The term, 'height gain' is introduced. Height gain, $G_{h_{b,a}}$, is defined as the relative received level when the SS antenna height is b (m) based on a (m). Here, $b > a$, the received level represents a 1-m high section mean value of the acquired data shown as plots in Fig. 2. Figure 3 shows the dependency on the BS-SS horizontal distance of the height gain at $h_{SS} = 10$ m based on $h_{SS} = 5$ m at $h_{BS} = 32$ m in the Suginami area, which includes the measured results shown in Figs. 2(a) and 2(b). The SS antenna height of 5 m corresponds to just above the rooftop of a one-story building, and 10 m corresponds to just above the rooftop of a second-story building. Figure 3 indicates that the height gain, $G_{h_{10m, 5m}}$, depends on the BS-SS horizontal distance, and the height gain tends to be large in the relatively far region rather than those in the relatively near region.

3. PROPAGATION MECHANISMS CAUSING HEIGHT VARIATION DEPENDENCY ON LOCAL SS CONDITIONS

3.1 Calculation of Height Variation of Path Loss at SS

The variation in the path loss according to the SS antenna height and multipath wave components arriving at the SS antenna were calculated based on GO and UTD to reveal the propagation mechanisms that cause the height variation dependency on the local SS conditions.

The assumed propagation model is shown in Fig. 4. Here, w is the building spacing, and h_1 and h_2 are the building heights. The calculated arrival waves at the SS antenna are the direct wave (only in the LOS region), one-time to eight-time regular reflected waves from the building walls, one-time diffracted waves due to the corners of the rooftops of buildings, and one-time diffracted and reflected waves from the corners of the rooftops and walls of the buildings. For simplicity, only two neighboring buildings are considered and each building is approximated as rectangular bodies. For calculations of the diffracted waves, the UTD for metal edges is used. For calculations of the reflection coefficients on the walls of buildings, a complex permittivity of $6.95 - j0.74$ (that of concrete at 5 GHz) [13] is used.

3.2 Calculation Results and Discussion

The calculated results using the model employing GO and UTD mentioned above for different local conditions (especially, incidence angle θ) of a SS are shown in Figs. 5(a) and 5(b) with the measured results shown in Figs. 2(a) and 2(b). Both the calculated and measured results shown in Figs. 5 are normalized by letting the average level of the received power in the LOS region on the building roofs above approximately 2 m be 0 dB. Figure 5(a) shows the results in which the BS-SS horizontal distance is 330 m and $\theta = 4.06^\circ$, and Fig. 5(b) shows those for 1360 m of BS-SS horizontal distance and $\theta = 0.94^\circ$. The measured values are the averages of the power over a 1-m section in height.

The calculated results in Figs. 5(a) and 5(b) also indicate the contents of the arriving multipath waves. In these figures, (0) denotes the direct wave, (1)–(3) the 1 to 3-time reflected waves and (D) the once-diffracted wave. Although the once-diffracted waves arrive at any height of the SS antenna, there are restrictions on the height for the direct wave and the reflected waves. The lengths of the straight lines for (0)–(3) indicate the height ranges in which the respective wave can be received at the SS antenna. The calculated total level (power derived from the vector sum of the direct, reflected, and diffracted waves) agrees with the measured results in both Figs. 5(a) and 5(b).

Figure 5(a) shows that the one-time, two-time, and three-time reflected wave components represented by indexes (1) – (3) are dominant compared to the one-time diffracted wave component represented by index (D). In Fig. 5(a), the measured level agrees with the calculated level of the direct, one- and two-time reflected wave components at the minimum height where the direct, one- and two-time reflected waves arrive at the SS antenna, respectively. On the other hand, Fig. 5(b) shows that the arrival region of the regular reflected waves represented by indexes (1) – (3) is very short and the one-time diffracted wave component represented by index (D) is dominant compared to these regular reflected waves. In addition, the height variation of the total level is nearly equal to that of the one-time diffracted wave.

These results show that a change in the height variation characteristics is caused by the difference in composition of the arriving waves at the SS antenna. In other words, whether or not the regular reflected waves have a level higher than the one-time diffracted wave when arriving at the SS strongly influences the height variation characteristics of the path loss.

Figure 6 shows the mechanism of the propagation over the rooftops based on a geometrical propagation model. We can divide the height variation of the path loss due to the BS-SS horizontal distance into the following three regions depending on the arriving wave dominant to the entire level.

- (a) The direct wave dominant region where the BS-SS horizontal distance is very short.

In this region, the direct wave can arrive at any height of the SS antenna. The path loss and the height variation of the path loss at the SS are dominated by the propagation loss of the direct wave.

- (b) The reflected wave dominant region where the BS-SS distance is relatively short.

In this region, a strong reflected wave as a one- or two-time reflected wave and diffracted wave can arrive at any height of the SS antenna in the NLOS region. The propagation loss of the minimum-time-reflected wave arriving at any height of the SS antenna is smaller than that of the diffracted waves in the NLOS region. The path loss and height variation of the path loss at the SS in this region are dominated by the reflected waves. The path loss in the relatively near region corresponds to the direct, one-, and two-time reflected wave components at the minimum height where the direct, one- and two-time reflected waves arrive at the SS, respectively.

- (c) The diffracted wave dominant region where the BS-SS distance is relatively long.

In this region, a strong reflected wave as a one- or two-time reflected wave can only just arrive at the SS antenna in NLOS region where the SS antenna height is lower than that of the surrounding buildings, and only weak many-time-reflected waves and diffracted waves can arrive at the SS antenna. The propagation loss of the minimum-time-reflected wave arriving at the SS becomes larger than that of the diffracted wave. The path loss and height variation of the path loss at the SS in the far region are dominated by the diffracted waves from the edge of the building roof. The path loss and height variation of the path loss at the SS nearly correspond to that of the diffracted wave.

In the next section, we describe a new simple model for the height variation of the path loss reflecting the local conditions around the SS in terms of the arrival conditions of regular reflected and one-time diffracted wave components.

4. MODELING OF HEIGHT VARIATION IN PATH LOSS REFLECTING LOCAL SS CONDITIONS

4.1 Height Variation Model for Path Loss Reflecting Local SS Conditions

The height variation of the path loss due to the local SS conditions, especially the BS-SS horizontal distance, can be divided into three parts in terms of the dominant wave as mentioned in the previous section. The height variation of the path loss in each part is expressed as follows.

(a) When the BS-SS horizontal distance is very short (LOS region)

The direct wave is a dominant influence on the height variation of the path loss at a SS, $L_h(h_{SS})$. Figure 7(a) shows the geometry for the calculation of the height variation of the path loss at a SS, and $L_h(h_{SS})$ is expressed as Eq. (1).

$$L_h(h_{SS}) \approx 20 \cdot \log \left\{ \frac{4\pi \sqrt{d^2 + (h_{BS} - h_{SS})^2}}{\lambda} \right\} \quad (1)$$

Here, λ is the wavelength.

(b) When the BS-SS horizontal distance is relatively short

The reflected waves are a dominant influence on the height variation of the path loss at a SS. Figure 7(b) shows the geometry for the calculation of the height variation of the path loss at the SS. Point A represents the boundary between the LOS and NLOS regions, and the path loss at Point A is defined as the reference level for the height variation of the path loss. Term $L_R(\Delta h_{SS})$ is expressed as the excess loss based on the path loss at Point A. Here, Δh_{SS} is the depth to the NLOS region from Point A of the SS antenna. As mentioned in the previous section (Fig. 5(a)), $L_R(\Delta h_{SS})$ corresponds to the excess loss of the direct, one-, and two-time reflected wave components at the minimum height where each wave component can arrive at the SS antenna. The depth to the NLOS region from Point A of the SS antenna, $\Delta h_{SS,k}$, and the excess loss of the k -time reflected wave, $L_R(\Delta h_{SS,k})$, at the minimum height of the SS antenna where the n -time reflected wave can arrive at the SS antenna are expressed as Eqs. (2a) and (2b).

$$\Delta h_{SS,k} = \begin{cases} \frac{k w \cdot (h_{BS} - h_b)}{d \sin \varphi - w_1} & (k : \text{Even}) \\ \frac{(k w - w_1 + w_2) \cdot (h_{BS} - h_b)}{d \sin \varphi - w_1} & (k : \text{Odd}) \end{cases} \quad (k = 0, 1, 2, 3, \dots) \quad (2a)$$

$$L_R(\Delta h_{SS,k}) \approx 20 \log \left(\frac{d_{kp}}{d_{0p} \cdot R^k} \right) \quad (2b)$$

Here, φ is the angle between the building row and the line of visibility/LOS, R is the reflection coefficient of the wall surface of the building in the microwave band and is specified as -8 dB as indicated in Ref. [14], and h_b is the average building height. In addition, in terms of the variables in Fig. 7(b), d_{kp} , which is the path length of k -time reflected waves, is geometrically given by Eq. (2c).

$$d_{kp} = \frac{1}{\sin \varphi_k} \cdot \sqrt{A_k^2 + \left\{ h_{BS} + \Delta h_{SS,k} - h_b + \frac{w_1 \cdot (h_{BS} - h_b)}{d \sin \varphi - w_1} \right\}^2} \quad (2c)$$

$$\varphi_k = \tan^{-1} \left(\frac{d \sin \varphi}{A_k} \cdot \tan \varphi \right)$$

$$A_k = \begin{cases} d \sin \varphi + k w & (k : \text{Even}) \\ d \sin \varphi + (k - 1) w + 2 w_2 & (k : \text{Odd}) \end{cases}$$

The path loss between the limiting height of the k -time reflected wave and that of the $k+1$ -time reflected wave is found to be subject to linear interpolation by Fig. 5(a). Hence, the path loss in the reflected wave region can be given by the following, obtained from linear interpolation using Eq. (2).

When $\Delta h_{SS,k} \leq \Delta h_{SS} < \Delta h_{SS,k+1}$

$$L_R(\Delta h_{SS}) = L_R(\Delta h_{SS,k}) + \frac{L_R(\Delta h_{SS,k+1}) - L_R(\Delta h_{SS,k})}{\Delta h_{SS,k+1} - \Delta h_{SS,k}} \cdot (\Delta h_{SS} - \Delta h_{SS,k}) \quad (k = 0, 1, 2, 3, \dots) \quad (3)$$

Figure 8 shows an example of the calculated results using Eq. (3) as the ratio of w_1 to w_2 is varied at several values of φ . Figure 8 indicates that the height pattern of the path loss variation at any φ fluctuates except for when the ratio of w_1 to w_2 equals one. The center of the fluctuations corresponds fairly well to the height pattern of the path loss variation when the ratio of w_1 to w_2 equals one. In this paper, we attempt to construct the height variation model of the path loss at the SS as simple as possible. Hence, for simplicity, both distance w_1 between the SS and the building on the BS side, and distance w_2 between the SS and the building on the BS side, and distance w_2 between the SS and the building on the other side of the BS are set to $1/2w$.

$$w_1 = w_2 \cong \frac{1}{2}w \quad (4)$$

(c) When the BS-SS horizontal distance is relatively large

The diffracted waves are a dominant influence on the height variation of the path loss at a SS. Figure 7(c) shows the geometry for the calculation of the height variation of the path loss at the SS. The once-diffracted wave from the building edge is dominant-arriving wave in this region. As the once-diffracted wave, let us consider the diffracted wave from the diffraction points α and β in Fig. 7(c). Hence, the excess loss in the NLOS region based on the path loss at Point A, $L_D(\Delta h_{SS})$ is expressed as follows.

As the once-diffracted wave, let us consider the diffracted wave from diffraction points α and β in Fig. 7(c). Hence, the excess loss in the NLOS region based on the path loss at Point A, $L_D(\Delta h_{SS})$ is expressed as follows.

$$L_D(\Delta h_{SS}) \approx -10 \cdot \log \left\{ \left(\frac{D_\alpha \cdot d_{0p}}{d_{\alpha,a} \cdot \sqrt{d_{\alpha,b}}} \right)^2 + \left(\frac{D_\beta \cdot d_{0p}}{d_{\beta,a} \cdot \sqrt{d_{\beta,b}}} \right)^2 \right\} \quad (5)$$

Here, Δh_{SS} is the depth to the NLOS region from Point A of the SS antenna, and D_α and D_β are the UTD diffraction coefficients. Although the UTD diffraction coefficient has polarization dependence, the diffraction coefficients used here are the averages of the results for vertical and horizontal polarizations. Terms $d_{\alpha,a}$ and $d_{\beta,a}$ are the distances from the BS antenna to diffraction points α and β , while $d_{\alpha,b}$ and $d_{\beta,b}$ are the distances from diffraction points α and β to the SS. These are given by

$$d_{\alpha,a} = \sqrt{\left\{ \sqrt{d^2 - \left\{ \frac{d \sin \varphi \cdot (h_{BS} - h_b)}{d \sin \varphi - w_1} - \Delta h_{SS} \right\}^2} - \frac{w_1}{\sin \varphi} \right\}^2 + (h_{BS} - h_b)^2} \quad (6a)$$

$$d_{\alpha,b} = \sqrt{\left(\frac{w_1}{\sin \varphi} \right)^2 + \left\{ \frac{w_1 \cdot (h_{BS} - h_b)}{d \sin \varphi - w_1} + \Delta h_{SS} \right\}^2} \quad (6b)$$

$$d_{\beta,a} = \sqrt{\left\{ \sqrt{d^2 - \left\{ \frac{d \sin \varphi \cdot (h_{BS} - h_b)}{d \sin \varphi - w_1} - \Delta h_{SS} \right\}^2} - \frac{w_2}{\sin \varphi_1} \right\}^2 + (h_{BS} - h_b)^2} \quad (6c)$$

$$d_{\beta,b} = \sqrt{\left(\frac{w_2}{\sin \varphi_1} \right)^2 + \left\{ \frac{w_1 \cdot (h_{BS} - h_b)}{d \sin \varphi - w_1} + \Delta h_{SS} \right\}^2} \quad (6d)$$

Distance w_1 between the SS and the building on the BS side, and distance w_2 between the SS and the building on the other side of the BS are set to $1/2w$ as well as when the BS-SS horizontal distance is relatively short.

Term $L_D(\Delta h_{SS})$ is the function of the variables, w , φ , θ , and f . The dependency of $L_D(\Delta h_{SS})$ on these variables is shown in Figs. 9(a), 9(b), 9(c), and 9(d), respectively. The figures indicate that the characteristics of $L_D(\Delta h_{SS})$ are logarithmic versus the depth to the NLOS region when Δh_{SS} is greater than 1 m, and the dependencies of $L_D(\Delta h_{SS})$ on w , φ , and θ are not so strong. The difference in $L_D(\Delta h_{SS})$ within the parameter range of $10\text{m} \leq w \leq 30\text{m}$, $20^\circ \leq \varphi \leq 90^\circ$, and $0^\circ \leq \theta \leq 5^\circ$ is less than approximately 6 dB as shown in Figs. 9(a)-9(c). On the other hand, the dependency of $L_D(\Delta h_{SS})$ on the frequency is not negligible as shown in Fig. 9(d). Therefore, for simplicity, an approximate equation, which represents the calculation values of $L_D(\Delta h_{SS})$ using Eq. (5) and contains only variable f , can be derived as Eq. (7).

$$L_D(\Delta h_{SS}) \approx \begin{cases} \{5.8947 \cdot \log(f) + 0.31519\} \cdot \Delta h_{SS}^{(-0.003559f + 0.65122)} & (0 \leq \Delta h_{SS} < 1) \\ \{3.7432 \cdot \log(f) + 19.245\} \cdot \log(\Delta h_{SS}) + 5.8947 \cdot \log(f) + 0.31519 & (1 \leq \Delta h_{SS} < 10) \\ 24.5 \cdot \log(\Delta h_{SS}) + 9.6379 \cdot \log(f) - 4.93981 & (10 \leq \Delta h_{SS}) \end{cases} \quad (7)$$

Equation (7) is derived as follows. First, the central values in each parameter range mentioned above are chosen with regard to street angle φ , distance w between the buildings, and angle θ . In other words, $w = 20$ m, $\varphi = 45$ deg., and $\theta = 2$ deg. Next, the calculation results of $L_D(\Delta h_{SS})$ using Eq. (5) using $w = 20$ m, $\varphi = 45$ deg., and $\theta = 2$ deg. at some frequencies within the range of 2 to 30 GHz are approximated as a power function of Δh_{SS} at $0 \leq \Delta h_{SS} < 1$ and a logarithmic function of Δh_{SS} at $1 \leq \Delta h_{SS}$ as follows.

$$L_D(\Delta h_{SS}) \approx \begin{cases} A \cdot (\Delta h_{SS})^B & (0 \leq \Delta h_{SS} < 1) \\ C \cdot \log(\Delta h_{SS}) + D & (1 \leq \Delta h_{SS}) \end{cases} \quad (8)$$

Here, A , B , C , and D are coefficients for approximated formulas. These coefficients are derived from the calculated values by the least squares method at each frequency. The coefficients depend on the frequency, and can be approximated as a function of f . The calculated results of Coefficients A and B are shown in Fig. 10(a), and that for Coefficients C and D are shown in Fig. 10(b). Coefficients C and D are considered to be divided into two parts, i.e., when $1\text{m} \leq \Delta h_{SS} < 10\text{m}$ and $10\text{m} \leq \Delta h_{SS}$. The solid circles and squares in Figs. 10(a) and 10(b) represent the values of the coefficients at each frequency derived from the calculated results. The solid and dashed lines in the figures represent a least squares regression line and are expressed as follows.

$$A = 5.847 \cdot \log(f) + 0.31519 \quad (9a)$$

$$B = -0.003559 \cdot f + 0.65122 \quad (9b)$$

$$C = \begin{cases} 3.7432 \cdot \log(f) + 19.245 & (1 \leq \Delta h_{SS} < 10) \\ 24.5 & (10 \leq \Delta h_{SS}) \end{cases} \quad (9c)$$

$$D = \begin{cases} 5.8947 \cdot \log(f) + 0.31519 & (1 \leq \Delta h_{SS} < 10) \\ 9.6379 \cdot \log(f) - 4.93981 & (10 \leq \Delta h_{SS}) \end{cases} \quad (9d)$$

The Eq. (7) can be derived from Eqs. (8) and (9).

Some calculation examples of Eq. (7) are shown in Fig. 11 with the calculation values obtained using the original Eq. (5).

The height variation in the excess loss to the total received level at the SS, $L(\Delta h_{SS})$, depends on the dominant (strong) waves (reflected waves or diffracted waves) as mentioned before. In addition, the excess loss due to the arriving reflected waves and the arriving diffracted waves in the NLOS region can be derived as $L_R(\Delta h_{SS})$ and $L_D(\Delta h_{SS})$, respectively. Therefore, $L(\Delta h_{SS})$ can be expressed as Eq. (10).

$$L(\Delta h_{SS}) \approx \min\{L_R(\Delta h_{SS}), L_D(\Delta h_{SS})\} \quad (10)$$

Examples of the calculation results are shown in Fig. 12(a), 12(b), and 12(c). The solid lines in these figures represent $L(\Delta h_{SS})$. The figures indicate that the relationship of the amount between $L_R(\Delta h_{SS})$ and $L_D(\Delta h_{SS})$ changes as the horizontal distance between the BS and SS, d , increases. In the near region, $d = 50$ m, $L_R(\Delta h_{SS})$ is less than $L_D(\Delta h_{SS})$, and $L_R(\Delta h_{SS})$ becomes $L(\Delta h_{SS})$. In addition, the dependency of $L(\Delta h_{SS})$ on the frequency corresponds to that of the reflected waves. So the frequency dependency is negligible in this region. On the other hand, in the far region, $d = 1000$ m, $L_R(\Delta h_{SS})$ is greater

than $L_D(\Delta h_{SS})$, and $L_D(\Delta h_{SS})$ becomes $L(\Delta h_{SS})$. The dependency of $L(\Delta h_{SS})$ on the frequency corresponds to that of the diffracted wave.

4.2 Expression of Height Variation Model for Path Loss Reflecting Local SS Conditions

The discussion is now summarized by model representations as follows.

$$L(\Delta h_{SS}) \approx \min\{L_R(\Delta h_{SS}), L_D(\Delta h_{SS})\} \quad (11)$$

When $\Delta h_{SS,k} \leq \Delta h_{SS} < \Delta h_{SS,k+1}$

$$L_R(\Delta h_{SS}) = L_R(\Delta h_{SS,k}) + \frac{L_R(\Delta h_{SS,k+1}) - L_R(\Delta h_{SS,k})}{\Delta h_{SS,k+1} - \Delta h_{SS,k}} \cdot (\Delta h_{SS} - \Delta h_{SS,k}) \quad (k = 0, 1, 2, 3, \dots) \quad (12a)$$

$$\Delta h_{SS,k} = \frac{2kw \cdot (h_{BS} - h_b)}{2d \cdot \sin \varphi - w} \quad (12b)$$

$$L_R(\Delta h_{SS,k}) \approx 20 \log \left(\frac{d_{kp}}{d_{0p} \cdot R^k} \right) \quad (12c)$$

$$d_{kp} = \frac{1}{\sin \varphi_k} \cdot \sqrt{(d \cdot \sin \varphi + kw)^2 + \left\{ h_{BS} + \Delta h_{SS,k} - h_b + \frac{w \cdot (h_{BS} - h_b)}{2d \cdot \sin \varphi - w} \right\}^2} \quad (12d)$$

$$\varphi_k = \tan^{-1} \left(\frac{d \sin \varphi}{d \sin \varphi + kw} \cdot \tan \varphi \right) \quad (12e)$$

$$L_D(\Delta h_{SS}) \approx \begin{cases} \{5.8947 \cdot \log(f) + 0.31519\} \times \Delta h_{SS}^{(-0.003559 \cdot f + 0.65122)} & (0 \leq \Delta h_{SS} < 1) \\ \{3.7432 \cdot \log(f) + 19.245\} \times 5.8947 \cdot \log(f) + 0.31519 & (1 \leq \Delta h_{SS} < 10) \\ 24.5 \cdot \log(\Delta h_{SS}) + 9.6379 \cdot \log(f) - 4.93981 & (10 \leq \Delta h_{SS}) \end{cases} \quad (13)$$

4.3 Comparison with Measured Data in Terms of Height Gain at $h_{SS} = 10$ m Based on $h_{SS} = 5$ m, $G_{h_{10m}, 5m}$

4.3.1 Measurement

The measurements for height variation of the path loss at the SS were carried out in the Suginami area in Tokyo and the Tsukuba area in Ibaraki prefecture in Japan. The measurement scenarios and features are shown in Table I. The areas are flat. It should be noted that these areas include many two-story houses. The subscriber station antenna height (h_{SS}) is changed from 4 m to 10 m continuously at each measurement point. The frequency is 2.2, 5.2, or 25.15 GHz (CW). Both the BS and SS antennas are omni-directional in the horizontal plane and the polarization is vertical. The measured height gain at $h_{SS} = 10$ m based on $h_{SS} = 5$ m, $G_{h_{10m}, 5m}$, is acquired from the 1-m section median value of the measured height variation of the received level.

Here, the height gain, $G_{h_{10m}, 5m}$, is used as an evaluation parameter for the height variation with respect to the received level.

4.3.2 Validation

Regardless of the SS location, the average value of h_{BS} , φ , w , and h_b for all measurement points in each scenario are given as calculation parameters. The calculation results of the height gain, $G_{h_{10m}, 5m}$, are acquired as follows. Term Δh_{SS} can be expressed using h_{SS} as shown in Eq. (14).

$$\Delta h_{SS} = h_b - h_{SS} - \frac{w(h_{BS} - h_b)}{2d - w} \quad (14)$$

Therefore, we can acquire the calculated value of $L(\Delta h_{SS})$ when $h_{SS} = 5$ m and 10 m using Eqs. (11)-(14). If Δh_{SS} becomes negative, that is, a LOS condition arises between the BS and SS antennas, -6 dB is given as the $L(\Delta h_{SS})$ regardless of the SS antenna height because $L(\Delta h_{SS})$ is normalized by the path loss at the boundary between the LOS and NLOS regions. The difference in $L(\Delta h_{SS})$ between when $h_{SS} = 5$ m and 10 m is defined as the height gain, $G_{h_{10m}, 5m}$. The measured results in the scenarios in Table I and calculation results using Eqs. (11) and (14) are shown in Figs. 13(a)-13(e).

The tendency for the BS-SS horizontal distance of the calculation results agrees with that of the measured results in all measurement scenarios. Figure 13(a) shows the height gain at both 2.2 and 5.2 GHz. Although the calculation results indicate that the height gain has a frequency dependency on the BS-SS horizontal distance, no clear difference in the measured results between 2.2 and 5.2 GHz is observed. It appears that the frequency dependency of the measured height gain between 2.2 and 5.2 GHz is negligible in comparison to the location dependency or measurement error. However, Fig. 13(b) shows the results at 5.2 and 25.15 GHz, and indicates a clear frequency dependency of the measured results as well as for the calculated results. These results in Figs. 13(a) and 13(b) indicate that there is a frequency dependency for the height gain on the BS-SS horizontal distance, and it becomes remarkable as the frequency difference becomes large. Figures 13(c), 13(d), and 13(e) show the results at 5.2, 2.2, and 25.15 GHz, respectively. Parameters such as h_{BS} , h_b , φ , and w in Figs. 13(c)-13(e) are different from those in Figs. 13(a) and 13(b). The results in all the figures show good agreement with the measured and calculated height gain.

Based on the above discussion, it can be said that this height gain model can represent the characteristics of the height gain reflecting the local conditions of the SS. In other words, the height gain depends on the frequency, local conditions around the SS, and the horizontal distance between the BS and SS in the microwave band.

5. Conclusion

A height variation model of the path loss for evaluating the height gain at a SS taking into consideration the local SS conditions, the horizontal distance between the BS and SS, and operating frequency in the microwave band was presented. The model assumes fairly homogeneous propagation environments in terms of the building conditions such as a residential area as an applicable area.

The propagation mechanism causing the dependency of the height variation characteristics of the received level at a SS on the SS location are clarified in terms of the GO using UTD. The difference in the composition of the arriving wave at the SS causes a change in the height variation characteristics of the path loss at a SS. The height variation characteristics strongly depend on whether or not regular reflected waves have a higher level than that of the one-time diffracted wave arrive at the SS.

There is no frequency dependency of the height variation of the path loss at the SS where the regular reflected wave components are dominant (relatively near region). On the other hand, the frequency dependency of the height variation of the path loss at the SS where the one-time diffracted wave component is dominant (relatively far region) is the same as that of the diffracted waves.

A representation of the model was shown, and the model was validated using measured data and the validity of the model was indicated.

This model is useful for the radio zone design of microwave band BWA systems operating under NLOS conditions, and for height gain estimation at mobile station antennas in mobile communications.

References

- [1] H. Bolcskei, A.J. Paulraj, K.V.S. Hari, R.U. Nabar, and W.W. Lu, "Fixed Broadband Wireless Access: State of the Art, Challenges, and Future Directions," IEEE Comm. Mag., vol. 39, Issue 1, pp. 100-108, Jan. 2001.
- [2] M. Danesh, J.-C. Zuniga, and F. Concilio, "Fixed Low-Frequency Broadband Wireless Access Radio Systems," IEEE Comm. Mag., vol. 39, Issue 9, pp. 134-138, Sept. 2001.
- [3] H. Sari, "Technical Challenges and Trends in Broadband Wireless Access at Frequencies between 2 and 11 GHz," IEEE ICTTA 2004, pp. LVII- LVIII, April 2004.

- [4] P. Soma, D.S. Baum, V. Erceg, R. Krishnamoorthy, and A.J. Paulraj, "Analysis and Modeling of Multiple-Input Multiple-Output (MIMO) Radio Channel Based on Outdoor Measurements Conducted at 2.5 GHz for Fixed BWA Applications," IEEE ICC 2002, vol. 1, pp. 272-276, April 2002.
- [5] S.Y. Tan, et al., "Microcellular communications propagation model based on the uniform theory of diffraction and multiple image theory," IEEE Trans. Antennas. Propag. Vol. 44, pp. 1317-1325, Oct. 1996.
- [6] European Cooperation in the Field of Scientific and Technical Research EURO-COST 231, "Urban Transmission Loss Models for Mobile Radio in the 900 and 1800 MHz bands," Rev.2, The Hague, Netherlands, 1991.
- [7] Rec. ITU-R P.1546-2: "Method for point-to-area predictions for terrestrial services in the frequency range 30 MHz to 3000 MHz," Volume 2005 P series, ITU, Geneva, Aug. 2005.
- [8] ANSI/IEEE Std 802.11, 1999 Edition (R2003), "Wireless LAN Medium Access Control (MAC) and Physical Layer (PHY) Specifications," IEEE, June 2003.
- [9] IEEE Std 802.16e-2005 and IEEE Std 802.16-2004/Cor1-2005, "Physical and Medium Access Control Layers for Combined Fixed and Mobile Operation in Licensed Bands," IEEE, Feb. 2006.
- [10] N. Kita, A. Sato, and M. Umehira, "A Path Loss Model with Height Variation in Residential Area Based on Experimental and Theoretical Studies Using a 5G/2G Dual Band Antenna," IEEE VTC 2000-Fall, vol. 2, pp. 840-844, Sept. 2000.
- [11] C.L. Hong, I.J. Wassell, G. Athanasiadou, S. Greaves, and M. Sellars, "Wideband channel measurements and characterization for broadband wireless access," IEE ICAP 2003, vol. 1, pp. 429-432, March 2003.
- [12] D.A. McNamara, C.W.I. Pistorius, and J.A.G. Malherbe, Introduction to The Uniform Geometrical Theory of Diffraction, AETECH HOUSE, 1990.
- [13] M. Lott, Y. Fifield, D. Evans, and S. Hulyalkar, "Radio Channel Characteristics for Typical Environments at 5.2 GHz," in ACTS Mobile Communication Summit, pp. 252-257, Aalborg, Denmark, Oct. 1997.
- [14] E.N. Bramley, and S.M. Cherry, "Investigation of microwave scattering by tall buildings," Proc. of IEE, Vol. 120, No. 8, pp. 833-842, Aug. 1973.

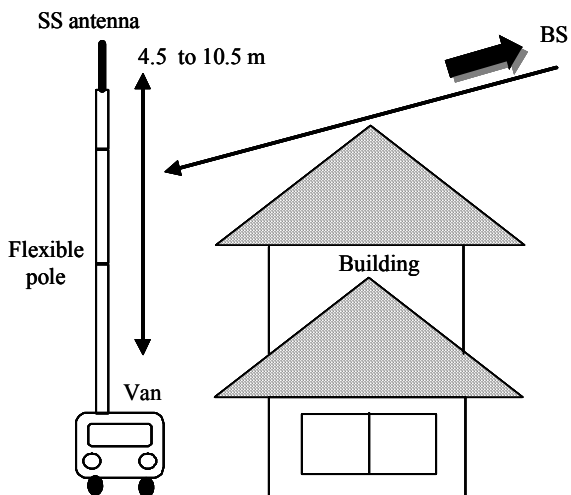


Fig. 1 Measurement method.



Picture 1 Measurement campaign.

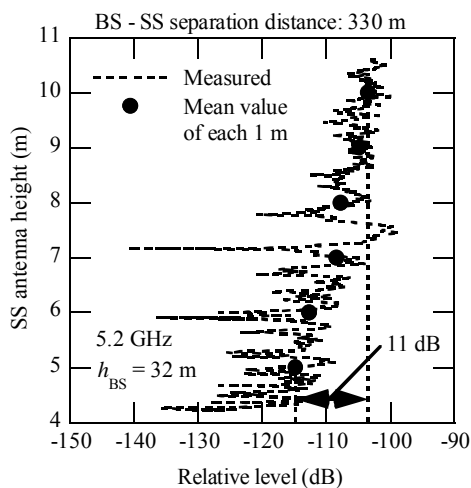


Fig. 2(a) Example of height variation characteristics. (In near region)

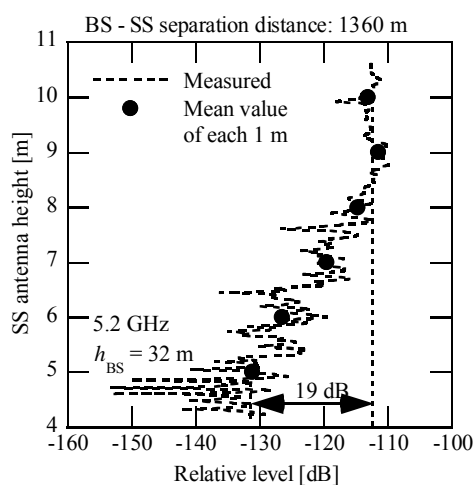


Fig. 2(b) Example of height variation characteristics. (In far region)

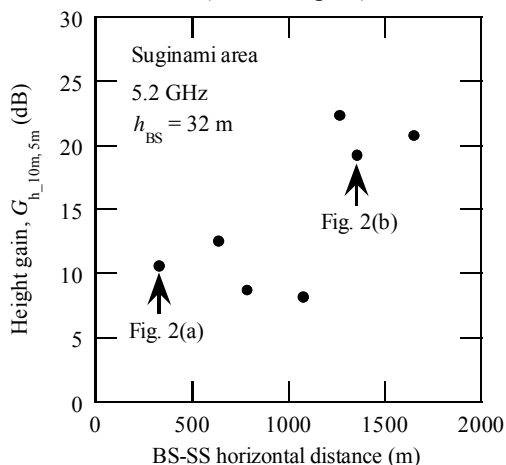


Fig. 3 Dependency on BS-SS horizontal distance of height gain at $h_{SS} = 10$ m (LOS) based on $h_{SS} = 5$ m (NLOS).

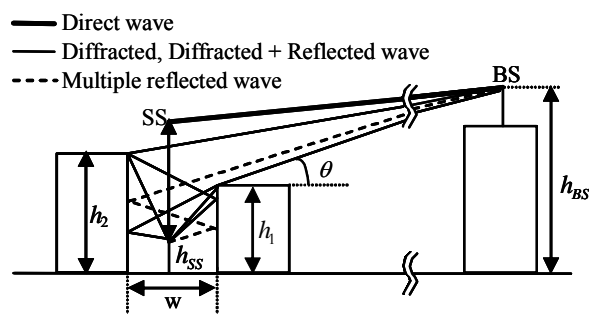


Fig. 4 Considered propagation model.

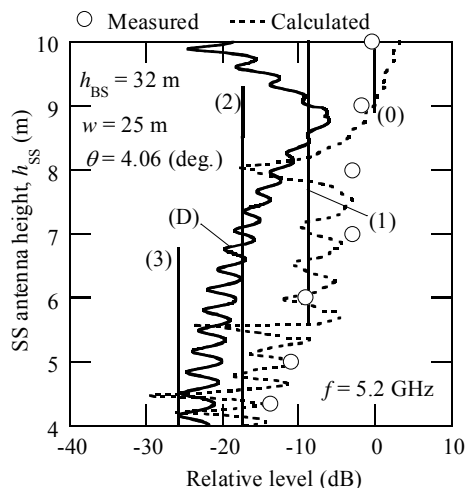


Fig. 5(a) Typical examples of comparison between calculated and measured results ($\theta = 4.06$ deg). (BS-SS horizontal distance = 330 m).

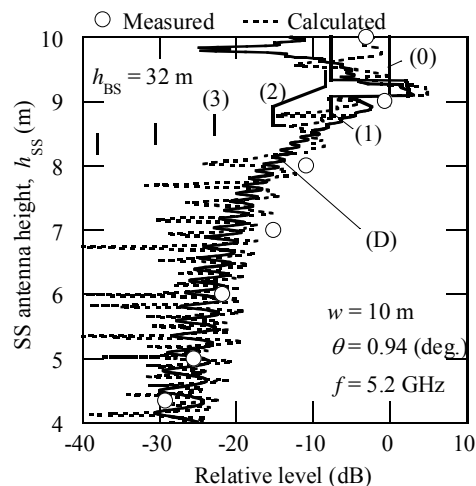


Fig. 5(b) Typical examples of comparison between calculated and measured results ($\theta = 0.94$ deg). (BS-SS horizontal distance = 1360 m).

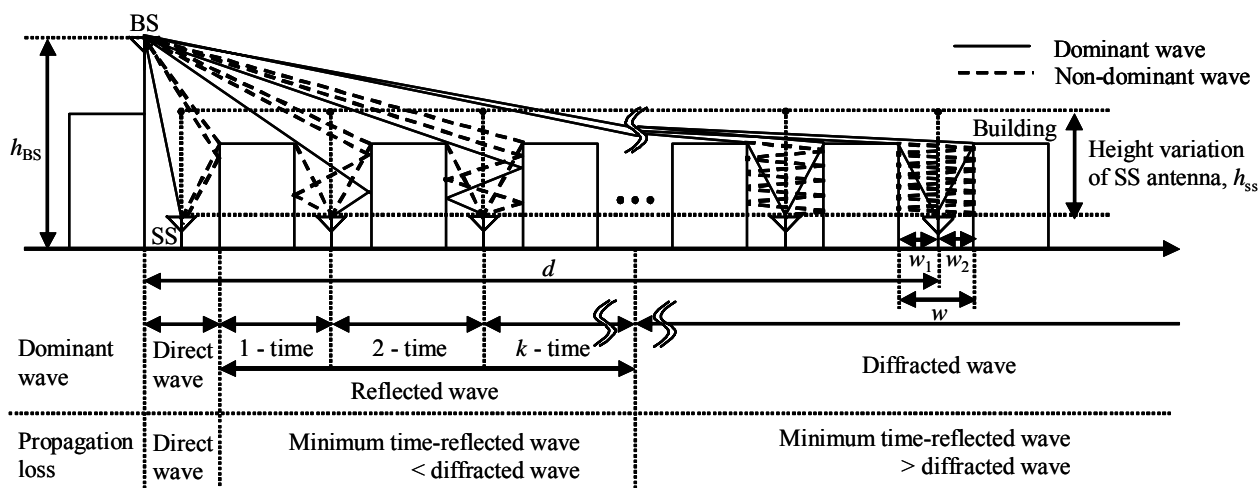


Fig. 6 Mechanism of propagation over rooftops based on geometrical propagation model.

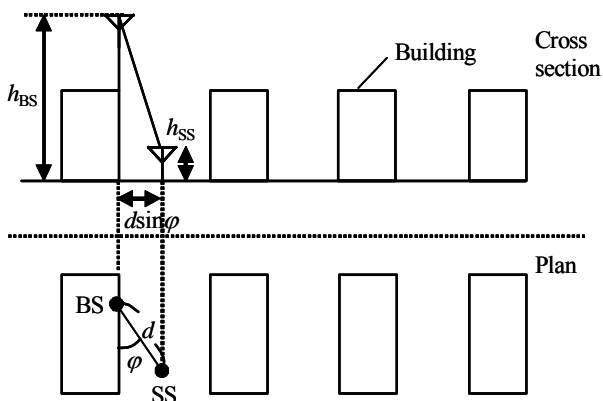


Fig. 7(a) Propagation model based on dominant waves that influence height variation of path loss.
- Geometry when the BS-SS distance is very short (LOS).

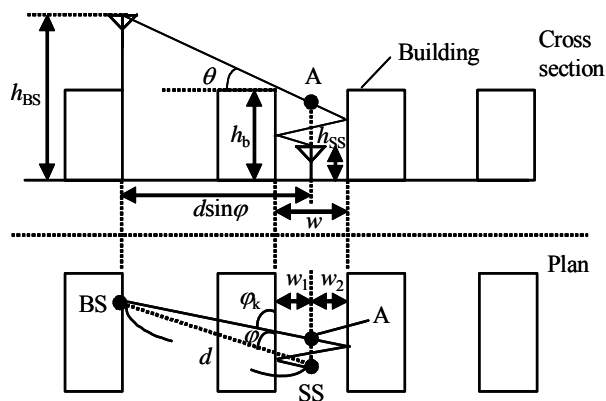


Fig. 7(b) Propagation model based on dominant waves that influence height variation of path loss.
- Geometry when the BS-SS distance is relatively short.

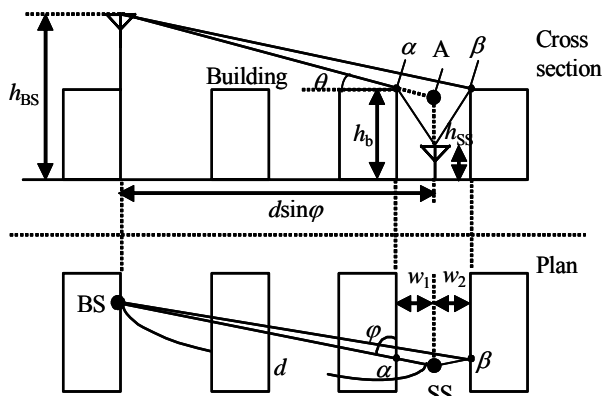


Fig. 7(c) Propagation model based on dominant waves that influence height variation of path loss.
- Geometry when the BS-SS distance is relatively long.

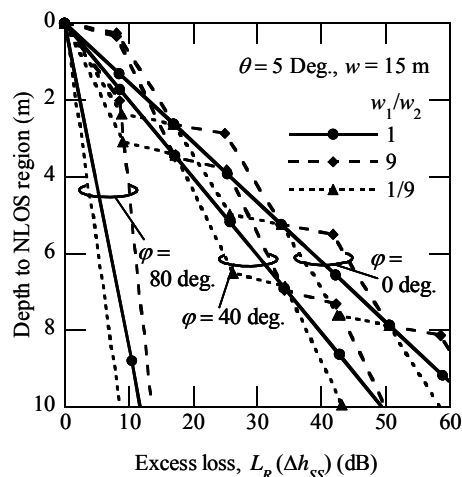


Fig. 8 Calculation examples of Eq. (3).

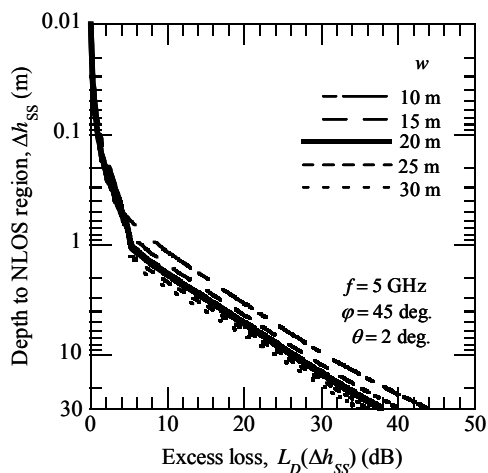


Fig. 9(a) Calculation examples of Eq. (5).
- Dependency on w

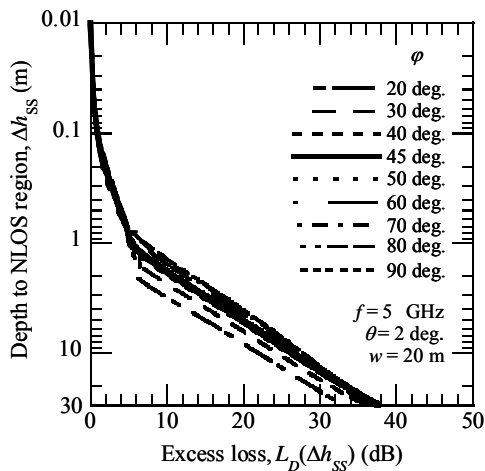


Fig. 9(b) Calculation examples of Eq. (5).
- Dependency on ϕ

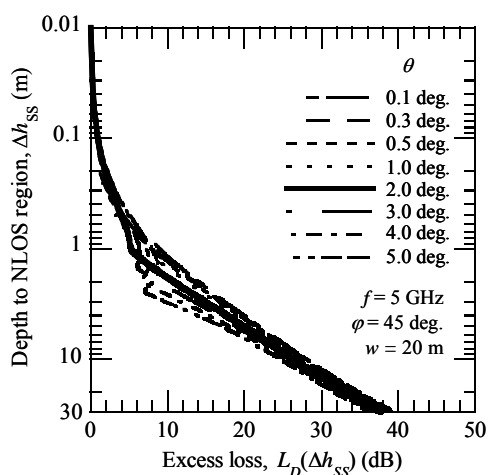


Fig. 9(c) Calculation examples of Eq. (5).
- Dependency on θ

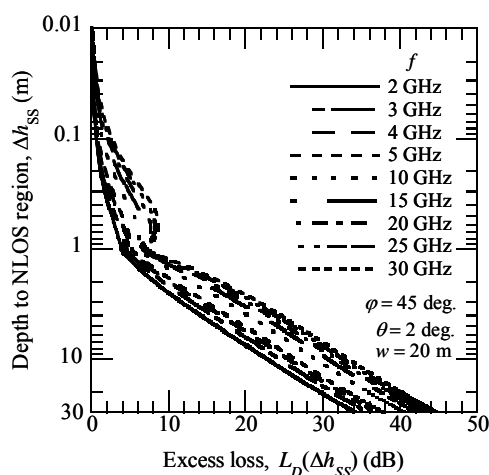


Fig. 9(d) Calculation examples of Eq. (5).
- Dependency on f

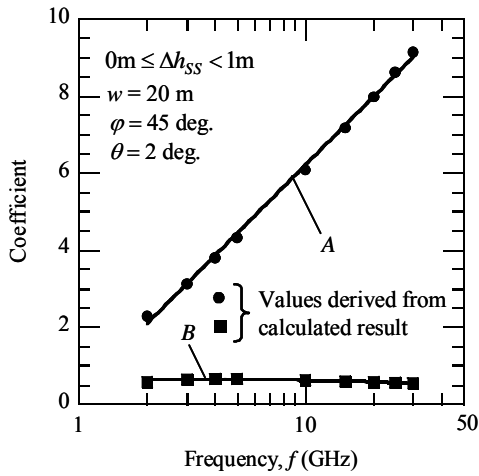


Fig. 10(a) Calculation results of coefficients.
- Dependency of coefficient A and B on frequency.

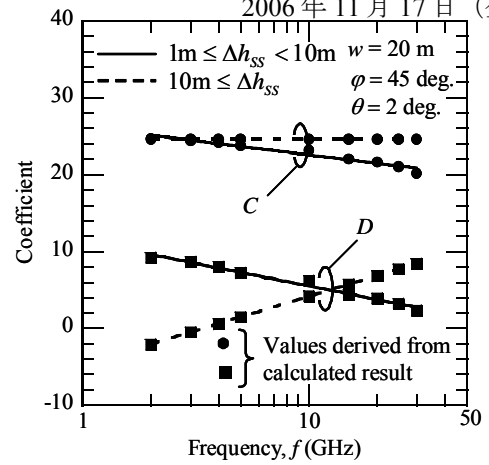


Fig. 10(b) Calculation results of coefficients.
- Dependency of coefficient C and D on frequency.

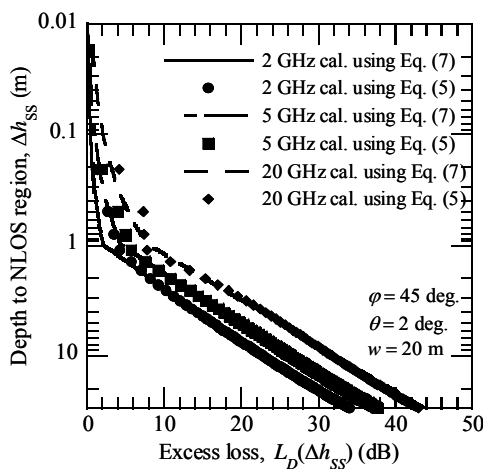


Fig. 11 Calculation example of Eq. (7).

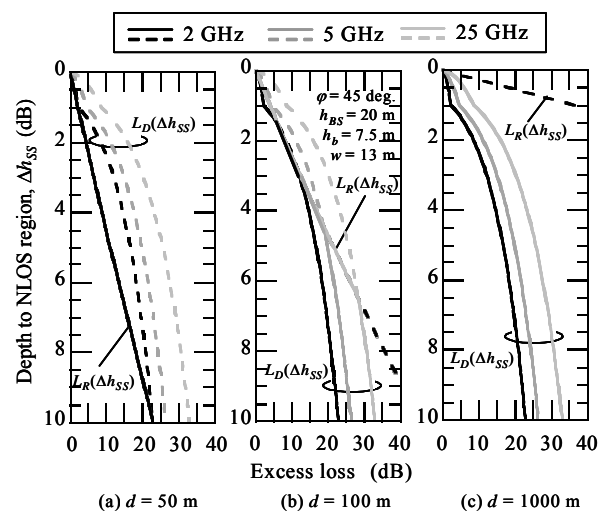


Fig. 12 Calculation examples for height variation of path loss at SS.

Table 1 Measurement scenarios and features

| Area | Suginami | | | | Tsu-kuba |
|--------------------------------------|------------|--------------|-----|-----|----------|
| | (a) | (b) | (c) | (d) | |
| BS antenna height, h_{BS} (m) | 18 | 20 | 21 | 32 | 15 |
| Average road angle, φ (deg.) | 38 | 56 | 45 | 44 | 28 |
| Average building separation, w (m) | 17 | 13 | 16 | 19 | 48 |
| Average building height, h_b (m) | 7.5 | 9.0 | 7.8 | 7.5 | 7.5 |
| Frequency (GHz) | 2.2 5.2 | 5.2 25.15 | 5.2 | 2.2 | 25.15 |
| Number of measurement points | 11 | 6 | 22 | 7 | 7 |
| ID, Fig. 13 | (a) | (b) | (c) | (d) | (e) |

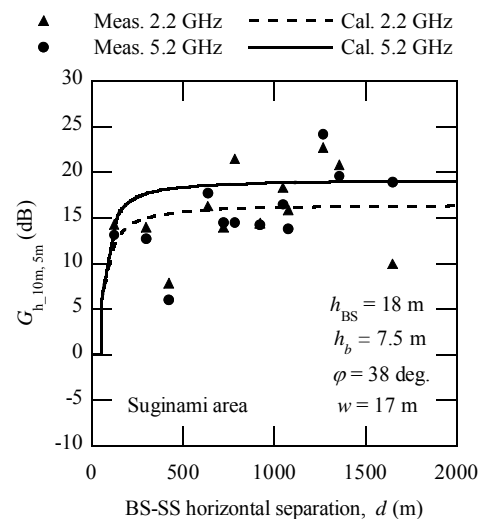


Fig. 13(a) Comparison between measured and calculated results.

- Suginami area ($h_{BS} = 18$ m, $f = 2.2$ and 5.2 GHz).

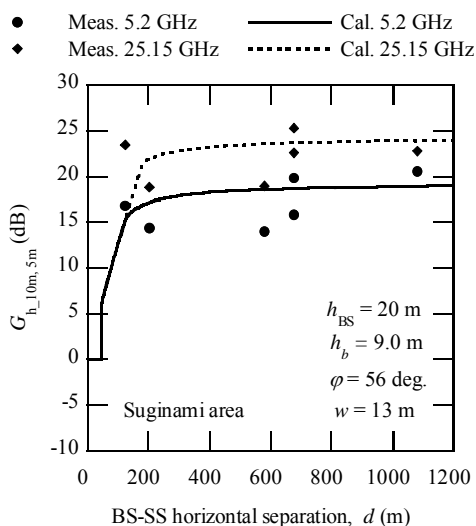


Fig. 13(b) Comparison between measured and calculated results.
- Suginami area ($h_{BS} = 20$ m, $f = 5.2$ and 25.15 GHz).

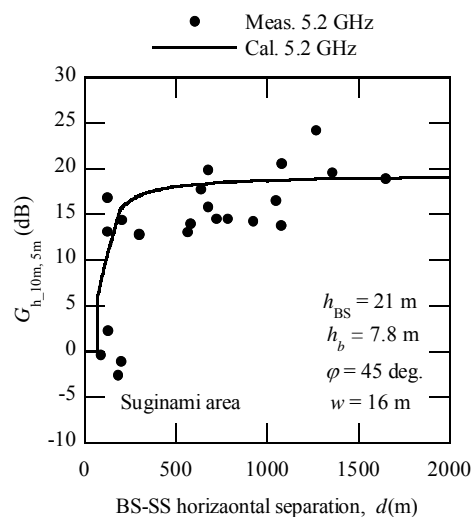


Fig. 13(c) Comparison between measured and calculated results.
- Suginami area ($h_{BS} = 21$ m, $f = 5.2$ GHz).

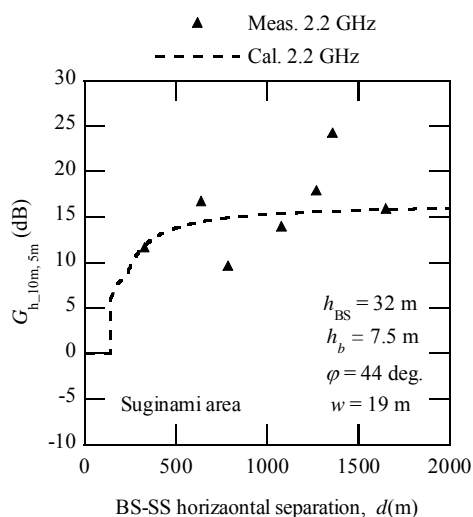


Fig. 13(d) Comparison between measured and calculated results.
- Suginami area ($h_{BS} = 32$ m, $f = 2.2$ GHz).

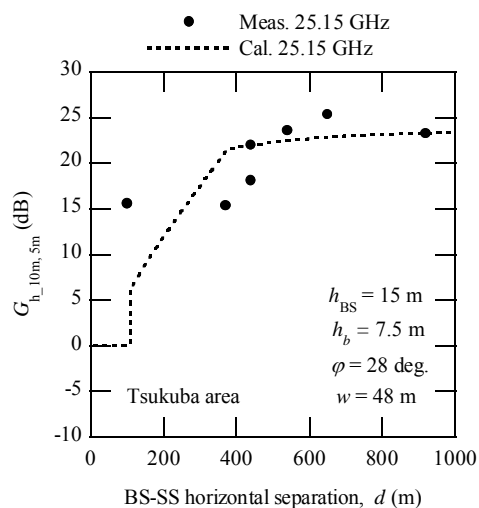


Fig. 13(e) Comparison between measured and calculated results.
- Tsukuba area ($h_{BS} = 15$ m, $f = 25.15$ GHz).